Iraqi Journal of Science, 2023, Vol. 64, No. 7, pp: 3679-3690
DOI: 10.24996/ijs.2023.64.7.43

ISSN: 0067-2904

Performance Estimation of Solar Imagery Using Different Types of Atmospheric Turbulence Models

Huda S. Ali
Department of Astronomy and Space, College of Science, University of Baghdad, Baghdad, Iraq

Received: 17/12/2022 Accepted: 27/3/2023 Published: 30/7/2023

Abstract

This paper proposed several approaches for estimating the optical turbulence of the Earth's atmosphere and their effect on solar images' resolution using ground-based telescopes based on von Kárman, Kolmogorov, and modified von Kárman PSDs models. The results showed a strong correlation coefficient for the modified von Kármán model of atmospheric representation. As can be seen in the case where solar adaptive optics have been properly designed, they typically decrease aberration considerably and provide greatly improved imagery.

Keywords: *Solar Image, Solar adaptive optics, Kolmogorov, von Kármán, Modified von Kármán.*

تقدير أداء الصور الشمسية باستخدام أنواع مختلفة من نماذج الاضطراب الجوي

هدى شاكر علي
قسم الفلك والفضاء، كلية العلوم، جامعة بغداد، بغداد، العراق

الخلاصه

في هذا البحث، تم اقتراح عدة طرق لتقدير الاضطراب البصري للغلاف الجوي للأرض وتأثيرها على دقة الصور الشمسية باستخدام التلسكوبات الأرضية بناءً على نماذج الكثافة الطيفية لقدرة فان كارمان وكولموكروف وفان كارمان المطور. اظهرت النتائج وجود معامل ارتباط قوي لنموذج فان كارمان المطور لتمثيل الغلاف الجوي. والذي يمكن رؤيته في الحالة التي تم فيها تصميم البصريات التكيفية الشمسية بشكل صحيح، وإنها تقلل الزيغ بشكل كبير وتوفر صورًا محسنة بشكل كبير.

1. Introduction

Solar observatory scientists have been working on the development of a new generation of adaptive optics for solar observations, which will help to provide a deeper understanding of the dynamics of the solar atmosphere and of the origin of solar storms in what is broadly called "space weather". In view of future implementations of the large telescopes, which have been aimed at research on a highly small scale, which show energetically highly significant magneto-hydrodynamic structure at every layer in the solar atmosphere, the pursuit of solar adaptive optics has been considered urgent [1][2].

*Email: hudashaker2000@gmail.com

The Earth's atmosphere distorts all observations of stars, planets, and the Sun made with ground-based telescopes, reducing the level of resolution achievable in remote object imaging and limiting the amount of information obtainable using standard optical techniques. Air turbulence, especially close to the ground, causes stars to twinkle at night and planets and the sun images to blur when observed at high magnification through a telescope. One of the most important advances in ground astronomy, which appeared near the end of the last century, has been the development of methods to correct the presence of the atmosphere – adaptive optics (AO) – that are utilized to push the image resolution toward its theoretical limit [3][4].

2. Turbulence of the atmosphere

It is widely known that the atmosphere of the Earth represents a typical random inhomogeneous medium containing two medium types: one of them represents discrete turbid atmospheric medium that consists of particles, and the second one represents "continuous" turbulent atmospheric medium that consists of molecules that are thermally moving. The first medium results in the attenuation of energy of the optical waves, which is the effect of attenuation. The other type of medium leads to effects of the atmospheric turbulence, like fluctuations of angle-of-arrival, scintillation of intensity, beam spread, beam wander, spot distortions, etc. [5].

Due to the fact that those optical phenomena are dependent upon the differential instead of the absolute optical path length values, spatial statistics are utilized for describing structure functions' random variations [6][7]. Structure function, mean square difference in refraction index, $n(r)$, between a pair of different locations in the space, $r_1$and r_2, is expressed in the form of [8]:

$$D_n(\boldsymbol{r}) = \langle |n(r_1) - n(r_2))|^2 \rangle \quad \text{.....(1)}$$

Where $\boldsymbol{r}$ is $r_1 - r_2$.

Now, over the inertial sub range, $l_o$and L_o, Kolmogorov's theory additionally establishes structure function according to structure constant values:

$$D_n(r) = \begin{cases} C_n^2\, r^{2/3} & l_o < r < L_o \\ C_n^2\, {l_o}^{-4/3} r^{2/3} & r < l_o \end{cases} \quad \text{.....(2)}$$

Structure constant, C_n^2, quantifies optical turbulence strength. A C_n^2 value, which is on 10-17m$^{-2/3}$ magnitude order, has been considered as weak turbulence, and strong values of turbulence are on an order of 10-13m-2/3.

Atmospheric measurement results showed that the turbulence structure in the atmosphere of the Earth consists of Kolmogorov turbulence at lower values and non-Kolmogorov turbulence at greater values. Until now, there have been two models for the structure of atmospheric turbulence in the Earth's atmosphere: (i) A 2-layer model, which is turbulence in the atmosphere of the Earth consists of the Kolmogorov turbulence in the troposphere and (-5) non-Kolmogorov turbulence (the non-Kolmogorov turbulence the refractive index spectrum is described by replacing the exponent (11/3) in the Kolmogorov spectrum by a different exponent,α where typically 3< α <5) in the stratosphere, which has been constructed based upon the observations of the early Earth's atmosphere [9]. Revised 2-layer model based upon consistency between function of the structure of the refractive index and power spectral density [10][11]; (ii) 3-layer model, which means, that turbulence in the atmosphere of the Earth consists of Kolmogorov turbulence in the boundary layer, (-10/3) non-Kolmogorov turbulence in the free atmosphere, and (-5) non-Kolmogorov turbulence in the stratosphere that all have the form below [12]:

$$\emptyset_{nB}(k,z) = 0.033 C_n^2(z)\, k^{-11/3} \quad \text{.....(3)}$$

$$\emptyset_{nF}(k,z) = 0.015 C_{nF}^2(z) k^{-10/3} \quad \text{.....(4)}$$

$$\emptyset_{nS}(k,z) = 0.0024C_{nS}^2(z)k^{-5} \quad \text{.....(5)}$$

Where z represents distance of propagation, varying from z = 0 to z = L.
k is the spatial wave number for the refractive index fluctuations spectrum.
C_n^2 represents Kolmogorov turbulent index of the parameter of the refraction structure in the boundary layer and it has a unit of $m^{-2/3}$.
C_{nF}^2 represents non-Kolmogorov turbulent index of refraction structure parameter in the free troposphere and it has a unit of $m^{-1/3}$.
C_{nS}^2 represents non-Kolmogorov turbulent index of refraction structure parameter in the stratosphere and it has a unit of m^{-2}.

Noticeably, the structure of the atmosphere's turbulence varies with different altitudes and atmospheric situations [13].
The diameter of atmospheric coherence r_o represents a more widely utilized parameter, and the phase PSDs for Kolmogorov, von Kárman, and the modified von Kárman are [14][15]:

$$\Phi_{\emptyset}^{K}(k) = 049r_0^{-5/3}\, k^{-11/3} \quad \text{... ... ... (6)}$$

$$\Phi_{\emptyset}^{vK}(k) = 049r_0^{-5/3}\,(k^2 + k_0^2)^{-11/3} \text{ ...} \quad \text{... ... . (7)}$$

$$\Phi_{\emptyset}^{mvK}(k) = 049r_0^{-5/3} \exp(-k^2/k_m^2)(k^2 + k_0^2)^{-\frac{11}{3}} \quad \text{... ... . (8)}$$

Where $\Phi_{\emptyset}^{\mathrm{K}}$, $\Phi_{\emptyset}^{\mathrm{vK}}$, and $\Phi_{\emptyset}^{\mathrm{mvK}}$ represent Kolmogorov, von Kárman, and the modified von Kárman refractive-index PSDs, respectively.
$k_m = 5.92/ l_0$ and $k_0 = 2\pi/L_0$.

The values of k_m and k_0 are chosen to match the small-scale (high-frequency) and large-scale (low-frequency) behavior predicted by the dimensional analysis. The modified von Kárman is the simplest PSD model that includes effects of both inner l_0 and outer L_0 scales.

3. Imaging through atmospheric turbulence

The diffraction theory makes it relatively simple to describe how waves move through the atmosphere and into the focal plane of the telescope. A well-known Fourier correlation between the amplitude of an electro-magnetic wave in the telescope's pupil and the amplitude in the focal plane is created when optical components, like mirrors or lenses, are included in a spherical approximation, using notation $A(\vec{u})$ for complex amplitude in the focal plane and $\psi(\vec{x})$ for complex amplitude in the telescope's pupil. Both amounts have been connected via Fourier transformation where integration has been carried out over the telescope's pupil. The phase $\varphi(\vec{x})$ of $\psi(\vec{x})$ includes a turbulent atmosphere and telescope aberrations. In the focus of the telescope, the intensity distribution $I(\vec{u}) = |A(\vec{u})|^2$ is usually used and may be expressed as [16]:

$$I(\vec{u}) = \iint \psi(\vec{x}')\psi^*(\vec{x}'')\exp(2\pi i(\vec{x}'-\vec{x}'')\vec{u})d\vec{x}'d\vec{x}''$$
$$= \int\left(\int \psi(\vec{x}')\psi^*(\vec{x}'-\vec{x})d\vec{x}'\right)\exp(2\pi i\vec{x}\vec{u})d\vec{x} \text{.....(9)}$$

Where $\int \psi(\vec{x}')\psi^*(\vec{x}'-\vec{x})d\vec{x}'$ represents auto-correlation of amplitude in the telescope's people, which has been referred to as optical transfer function (OTF). OTF is a purely real

function that is roughly triangle-shaped when a plane wave from a point source at infinity enters a perfect, or aberration-free, telescope. The airy disk represents Fourier transformation of the diffraction-limited point spread function (PSF). The coherence function, also known as an ensemble average over all feasible realizations, could be used for expressing the autocorrelation in a situation of stochastic fluctuations of an electromagnetic wave caused by an incoherent source or by the atmospheric turbulence [17]:

$$\Lambda\left(\vec{x}\right) = \left\langle \psi\left(\vec{x}'\right)\psi * \left(\vec{x}'-\vec{x}\right)\right\rangle \ldots\ldots\ldots(10)$$

Connecting atmospheric characteristics to the function of coherence in the telescope's pupil and, consequently, to its Fourier transformation, PSF, in the focal plane of the telescope, is one of the fundamental goals of turbulence theory. The term "seeing disk" indicates PSF's FWHM, which occurs when atmospheric turbulence, instead of the diameter of the telescope, limits the size of PSF [18].

4. Adaptive optics techniques

Some factors make using adaptive optics in solar astronomy desirable, which include: (i) Spectroscopy, in which short durations of exposure and 1D spatial coverage make it impossible to use any other techniques for high-resolution observations with the necessary sensitivity levels. (ii) Routine observing, which demands the best image at all times due to the observation of an extremely time-variable solar atmosphere and the necessity to achieve maximal coverage of the solar active areas. Routine computer-intensive image reconstructions are not acceptable at this time. (iii) Coronal observation, which necessitates the employment of laser guide star technology due to the lack of a suitably luminous surface structure. A combination of image selection, adaptive optics, and post-detection techniques will be quite helpful in various situations, as has already been mentioned for image selection methods. With the use of image restoration approaches, residual image deterioration effects brought on by, for instance, an adaptive optics system that isn't entirely successful and anisoplanicity effects, can be eliminated [19].

5. Wave-front sensing techniques on extended objects

Compared to night AO, solar AO faces a number of different challenges, and solar AO systems are in some aspects more technically challenging than night AO. The main challenges are seeing the worst and changing time of day, as well as the fact that solar astronomers mostly observe at visible wavelengths and solar wavefront sensors, which must operate on low-contrast, extended, and time-varying objects like solar granules [20]. For the wave-front sensing, non-solar adaptive optics devices use points or points that resemble points. The main distinction between them and solar adaptive optics is the requirement for wave-front sensing on an extended, structured object (as seen in Figure 1). Sunspots and their small scale, sub-arcsecond structure, could also be utilized in solar active regions. Solar granulation is the most suitable structure of the solar surface that exists anywhere on the solar disk, has a typical 1.5" size, is visible in the broadband image, and has (wavelength-dependent) contrast that equals 5-10%. There are occasionally pores: very small sunspots with sizes close to one arcsecond. In such specific situation, the pore could be employed as the (inverse) point-like object and non-solar wave-front sensing techniques could be applied. Yet, in general, extended object wave-front sensing approaches must be developed [19] [22] [23][24].

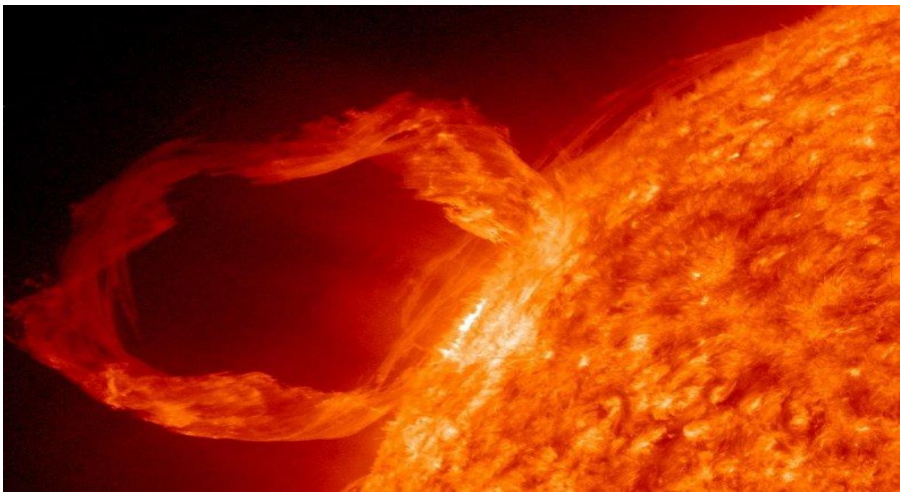

Figure 1: Solar surface structure [21].

6. Multi-conjugate adaptive optics (MCAO)

There have been a number of proposals to increase the size of the isoplanatic patch by using a number of adaptive mirrors placed at the confluences of different layers of the atmosphere. The technique requires that one first determines the full three-dimensional structures of the atmospheric wavefront deformation. This could, in principle, be done by "atmospheric tomography," which uses projections of ground-level wavefront distortions from arrays of laser-guiding stars, or, in the case of extended surface-structured objects such as the sun, by wavefront sensing on different parts of the body [25]. MCAO systems also require having several wave-front sensors coupled to guide stars in different directions within the field of view of interest in order to probe a larger portion of the turbulent volume [26].

7. An adaptive optics option for the observations of the solar corona

The solar adaptive optic systems are used on the solar disks, in which wave-front sensing is possible due to the solar surface structure. Such wave-front sensing is not feasible for solar corona observations. In the case of viewing this faint ring around the sun, the radiation from the faint solar corona (about 1 millionth the brightness of the solar disk) is obscured by a background of scattered light caused by aerosol and Rayleigh scattering in the atmosphere as well as scattering within the coronagraph. Since such stars will be moving at a 0.04arcsec/sec rate due to the Earth's rotation around the sun, the total amount of time for observation is only a few minutes for each coronal point [19]. In case the European Solar Telescope is implementing an adaptive secondary mirror, a pitch less than 20 mm would be required to accommodate all actuators within a 800 mm mirror [27].

8. Zernike circle polynomials

We describe a representation that is complete and orthogonal, since it is preferable to be utilized when aberrations get complex. Over a circular aperture, Zernike circle polynomials have been found orthogonal and complete. Zernike circle polynomials can be defined according to a number of conventions and ordering systems; in such conventions, polynomials can be defined as [28][29] [30]:

$$Z_n^m(\rho,\theta) = N_n^m R_n^{|m|}(\rho)\cos(m\theta) \quad \text{for } m \geq 0,\ 0 \leq \rho \leq 1,\ 0 \leq \theta \leq 2\pi$$
$$= -N_n^m R_n^{|m|}(\rho)\sin(m\theta) \quad \text{for } m < 0,\ 0 \leq \rho \leq 1,\ 0 \leq \theta \leq 2\pi$$

for a given n: m can only take on values of $-n, -n+2, -n+4, \ldots, n$ ……..(11)

N_n^m is the normalization factor

$$N_n^m = \sqrt{\frac{2(n+1)}{1+\delta_{m0}}} \qquad \delta_{m0} = 1 \text{ for } m = 0, \quad \delta_{m0} = 0 \text{ for } m \neq 0 \qquad \text{……..(12)}$$

……..(13)

$R_n^{|m|}(\rho)$ is the radial polynomial

$$R_n^{|m|}(\rho) = \sum_{s=0}^{(n-|m|)/2} \frac{(-1)^s (n-s)!}{s!\left[0.5(n+|m|)-s\right]!\left[0.5(n-|m|)-s\right]!} \rho^{n-2s}$$

With modes defined entirely, any wave-front, $W(r,\theta)$) could be represented by Zernike series with coefficients a_i which is expressed as [31]:

$$W(r,\theta) = \sum_{i=1}^{\infty} a_i Z_i(r,\theta) \qquad \ldots\ldots\ldots (14)$$

The Zernike coefficients' squares could be added to determine the wavefront variance. This is a major practical advantage of describing aberrations with an orthogonal basis set [31].

$$\sigma^2 = \sum_{i=2}^{\infty} a_i^2 \qquad \ldots\ldots\ldots (15)$$

9. Numerical simulation based on Kolmogorov turbulence theory and results

The phase screen was generated based on a PSD function that was mentioned in equation (8) for the modified von Kármán mode for a circular aperture with a specified diameter.

A) Our numerical simulation gave MATLAB code for the generation of the phase screens utilizing Fast Fourier Transform (FFT) method as follows:

1. Generating a circular aperture (512x512 pixel) for a telescope with a specified diameter. See Figure (2).

Preliminary grid setup and constants were established, such as the number of sample points, physical size of grid, grid spacing, frequency mesh grid, wavelength, wave number, inner scale, outer scale, and Fried coherent diameter.

2. Simulated power spectral density for the modified von Kárman mode of atmospheric turbulence, see Figure (3).
3. The power spectral density's square root was calculated.
4. Zeroed out the phase's zero-frequency component.
5. Created a random Fourier coefficient draw.
6. The phase screen was then created with the use of FFT utilizing random draws. It must be noted that the inverse FFT's imaginary and real components resulted in two uncorrelated phase screens. Discarded the imaginary part and utilized the phase screen from the real part.

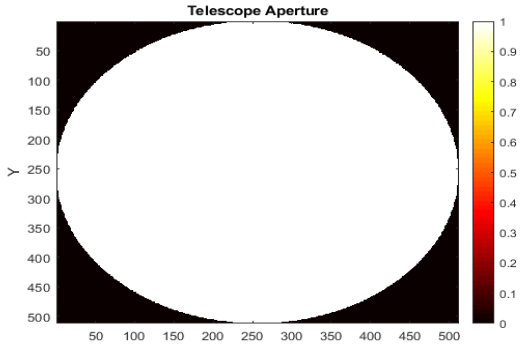

Figure 2: Telescope aperture

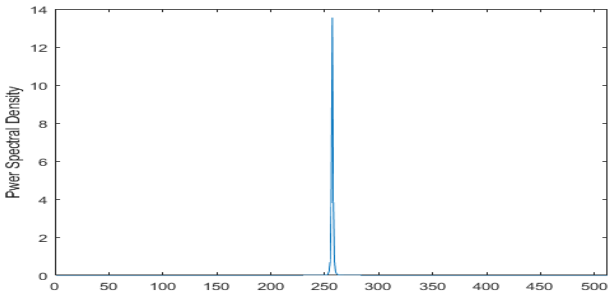

Figure 3: Power spectral density for the modified von Kármán mode

The phase screen was fitted to the apertures, as shown in Figures (4-5).

B) The solar image should be convolved with the 2D spatial impulse response of the imaging device in order to create a diffraction image:

a) The point spread function (PSF) for an ideal telescope and a perturbed telescope, using the above phase screen as atmospheric turbulence, were calculated by taking FFT of the optical

b) system (telescope) then multiplying it by the PSF conjugate, see Figures (6-7).

c) FFT for the extended object (solar image) was taken.

d) FFT for PSFwith and without turbulence was calculated.

e) Finally, the convolution process in frequency domain can be done by taking the dot product of the output in the previous b and c steps.

f) The absolute inverse FFT of the convolved images represented the diffraction image in the image plane, see Figures (8).

C) Establish a MATLAB function to calculate Zernike aberration modes using equation (11), given the mode number for each aberration type in normalized polar coordinates on the unit circle, such as piston, tip, tilt, defocus, astigmatism, and so on, see Figure (9).

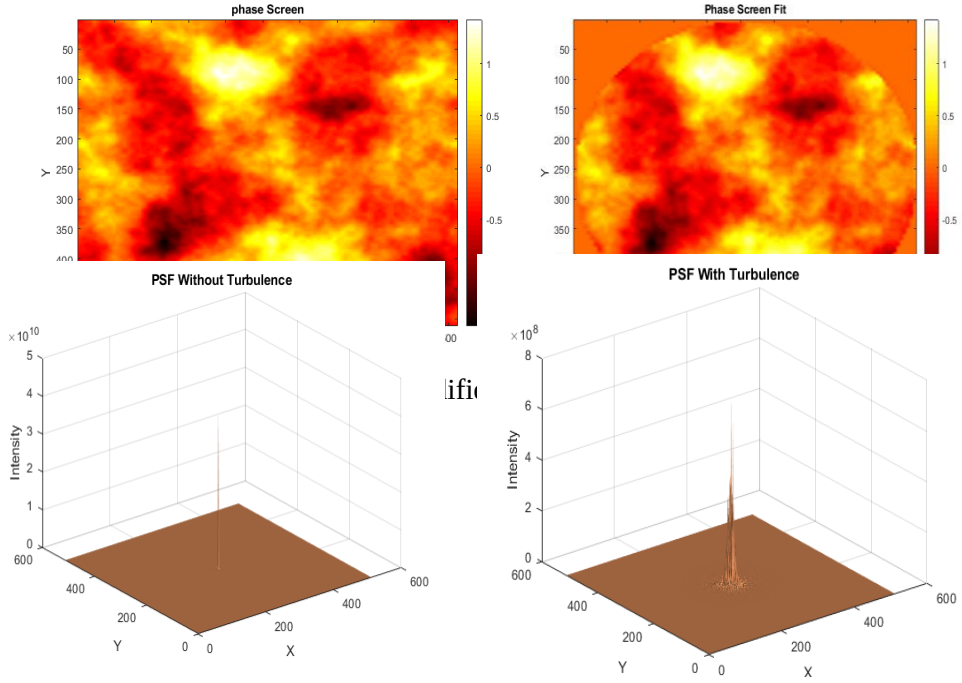

Figure 6: PSF without turbulence

Figure 7: PSF with turbulence

D) After generating a random draw of atmospheric turbulent using modified von Kármán mode, reconstruct the topology data from the computed limited version of Zernike aberration modes (4, 20, 50, and 110 modes) and compare it to the original phase screen as shown as in Figure (10).

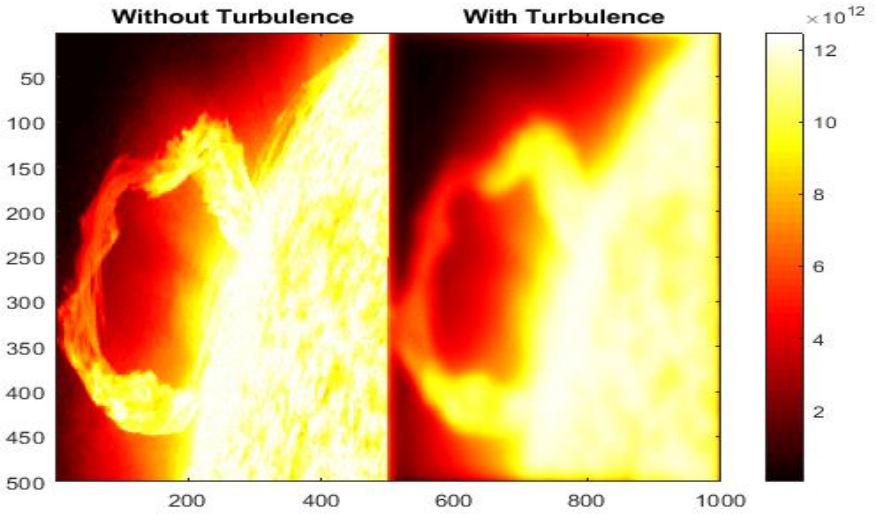

Figure 8: Original and blurred images

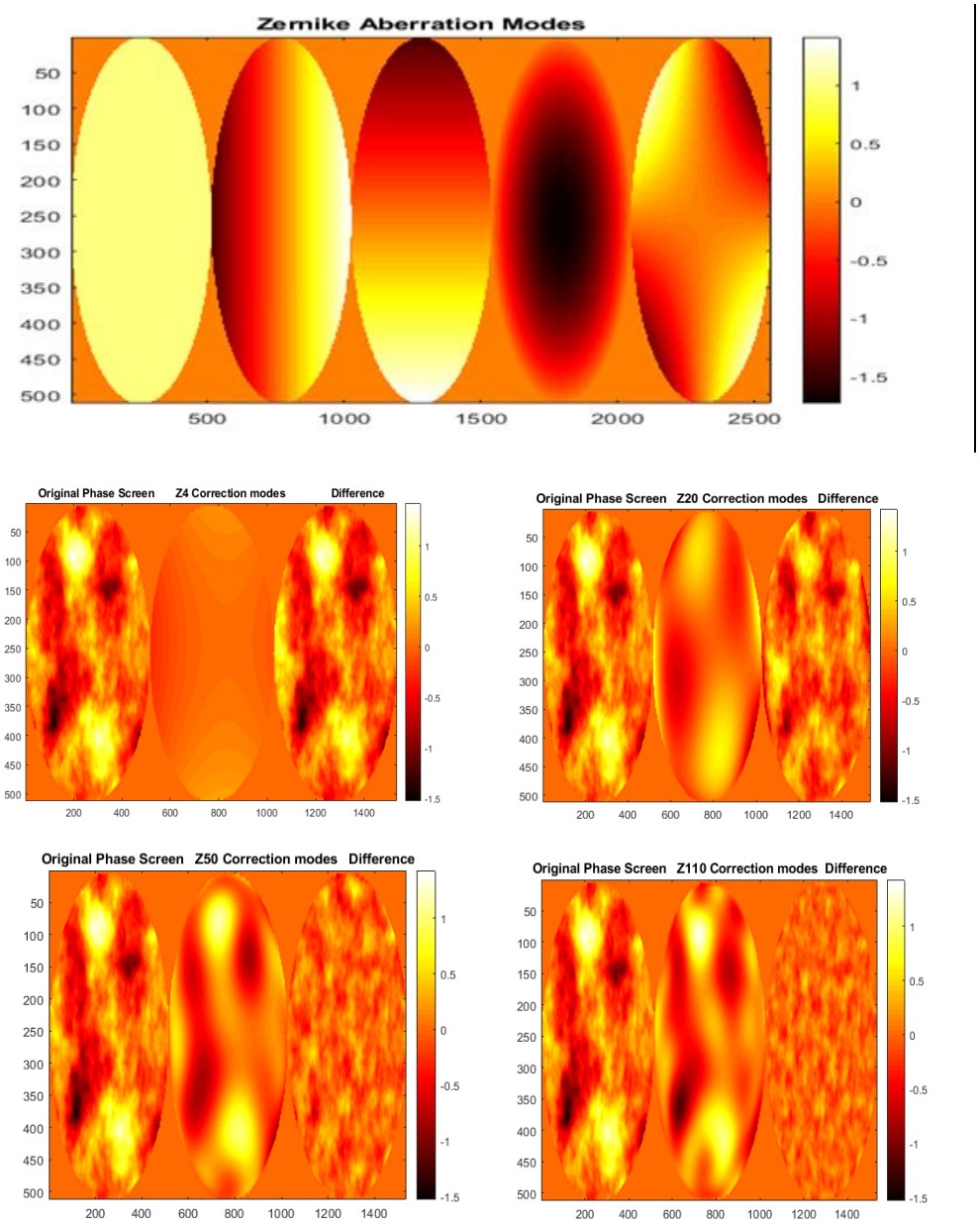

Figure 10: Phase reconstruction for each one from left to right represents original phase screen, Zernike aberration correction modes, and residual phase error (Difference)

Figure 9: Zernike aberration modes; Piston, Tip, Tilt, Defocus, Astigmatism

Due to the fact that more modes have been included in the representation of the Zernike series, see how the mode-limited version becomes more and more similar to the original aberration. Examining the mode-limited aberrations' residual phase is equally fascinating. Consider the complement regarding mode-limited aberrations as the difference between the created phase and the original (third column in Figure 10). Observe the way that the structures in the residual phase become more refined when more modes have been represented by the Zernike series.

E) The same procedure was done for generating the phase screens for the other turbulence models: Kolmogorov and von Kármán, as shown in Figure (11).

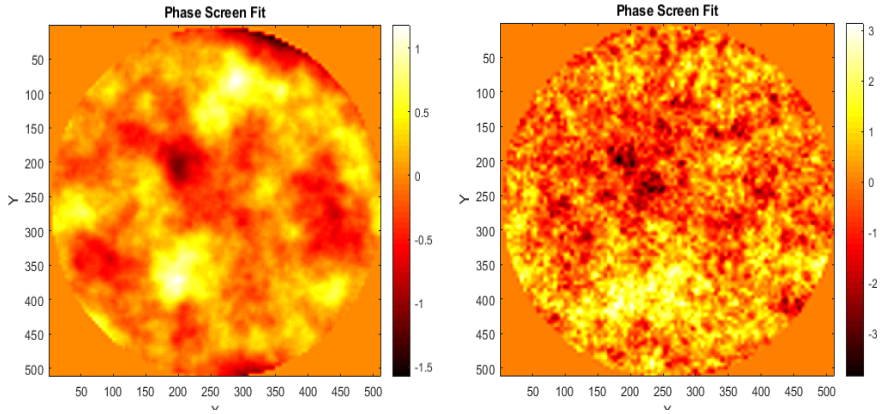

Figure 11: Phase screen for von Kármán and Kolmogorov models,

F) To quickly assess the quality of results, the spatial statistics were conducted for describing the random variations of structure functions such as variance, covariance, and correlation coefficient, see Figures (12-14).

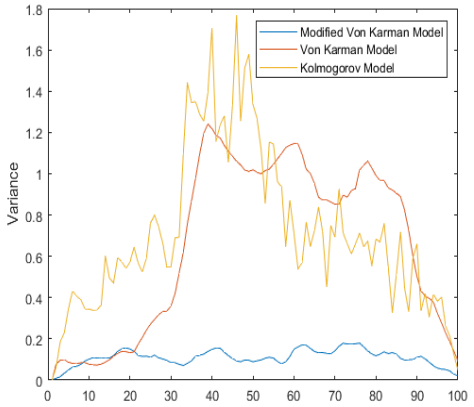

Figure 12: Variance statistical estimation

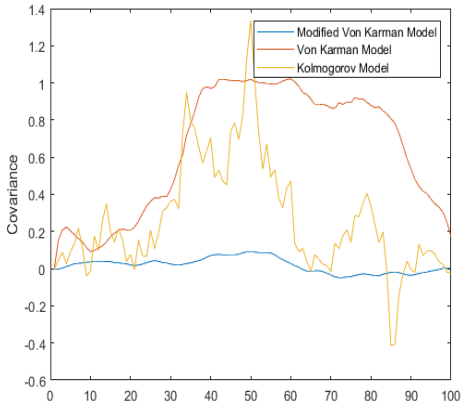

Figure 13: Covariance statistical estimation

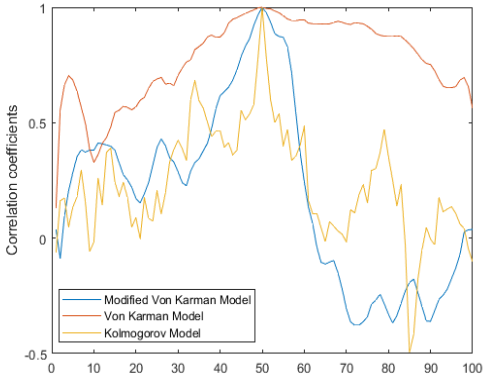

Figure 14: Correlation coefficient estimation

10. Conclusion

In this paper, several approaches for estimating the optical turbulence of the Earth's atmosphere and their effect on solar imagery using different types of atmospheric turbulence models were proposed, based on von Kárman, Kolmogorov, and the modified von Kárman PSDs. Estimation performance for random variations of structure functions of these models was done using statistical calculations, such as variance, covariance, and correlation coefficient.

From Figure 10, which reconstructs the phase screen from the computed limited version of Zernike aberration modes (4, 20, 50, and 110 modes), it is noticeable how the mode-limited version increasingly resembles the original aberration as more modes are included in the Zernike series representation.
Figures (12-14) show the enhanced correlation of the modified von Kármán model compared with other models.

The results showed that when solar adaptive optics are correctly built, the aberration is typically dramatically reduced and the imagery is greatly enhanced.

References

[1] T. R. Rimmele, M. Warner, S. L. Keil, P. R. Goode, M. Knölke, et al., "The Daniel K. Inouye Solar Telescope - Observatory Overview," *Solar Physics*, vol. 295, no. 12, , pp. 1-49, 2020.

[2] D. Schmidt, T. R. Rimmele, an, N. Gorceix, "Wavefront Sensing and Adaptive Optics For Solar Prominences,**"** *Proceedings of the SPIE*, vol. 10703, id. 803808, pp. 35- 47, 2018.

[3] R. L. Fante, "Electromagnetic beam propagation in turbulent media: an update," *Proceedings of the IEEE*, vol. 63, no. 12 , pp. 1424-1443, 1980.

[4] M. K. Mirdan, R. N. Hassan, and B. Q. Al-Aboodi, "Performance Simulation for Adaptive Optics Technique Using OOMAO Toolbox," *Karbala International Journal of Modern Science*, vol. 8, no. 3, pp. 306-312, 2022.

[5] C. A. Larry, and L. P. Ronald, "Laser Beam Propagation through Random Media," 2nd, *SPIE Optical Engineering Press, Washington, United States*, pp. 87-94, 2005.

[6] S. Basu, J. Osborn, P. He, and A. W. DeMarco, "Mesoscale modelling of optical turbulence in the atmosphere: the need for ultrahigh vertical grid resolution," *Monthly Notices of the Royal Astronomical Society*, vol. 497, no. 2, pp.2302-2308, 2020.

[7] M. Xu, S. Shao, N. Weng, L. Zhou, Q. Liu, and Y. Zhao, "Atmospheric Optical Turbulence Characteristics over the Ocean Relevant to Astronomy and Atmospheric Physics," *Applied Sciences*, vol. 11, no. 22, pp. 10548-10561, 2021.

[8] A. Y. Shikhovtsev, P. G. Kovadlo, E. A. Kopylov, M. A. Ibrahimov, S. A. Ehgamberdiev, and Y. A. Tillayev, "Energy Spectra of Atmospheric Turbulence for Calculating Parameter. I. Maidanak and Suffa Observatories in Uzbekistan. Atmosphere," *Atmosphere*, vol.12, no. 12, pp. 1614-1634, 2021.

[9] A. S. Gurvich, and M. S. Belen'kii , "Influence Of Stratospheric Turbulence On Infrared Imaging," *Journal of the Optical Society of America A*, vol. 12, no. 11, pp. 2517 – 2522, 1995.

[10] C. Ming, G. Taichang, H. Shuai, Z. Qingwei, L. Lei, and L. Gang "Simulating Non-Kolmogorov Turbulence Phase Screens Based On Equivalent Structure Constant And Its Influence On Simulations Of Beam Propagation," *Results in Physics*, vol. 7, Pages 3596-3602, 2017.

[11] A. P. Daniel, "Experimental Characterization Of Atmospheric Turbulence Supported By Advanced Phase Screen Simulations," *Ph.D. thesis, University of Maryland, College Park, United States*, pp. 39-51, 2020.

[12] W. Fazhi, D. Wenhe, Q. Yuan, L. Daosen, and F. Shuang, "A Survey of Structure of Atmospheric Turbulence in Atmosphere and Related Turbulent Effects," *Atmosphere*, vol. 12, no. 12, pp. 1608-1622 , 2021.

[13] V. S. Gudimetla, R. B. Holmes, T. C. Farrell, and *J. Lucas*, "Phase Screen Simulations Of Laser Propagation Through Non-Kolmogorov Atmospheric Turbulence," *Proceedings of the SPIE*, vol. 8038, id. 803808, pp. 8-20, 2011.

[14] M. Cubillos, and E. Jimenez, "Numerical Simulation Of Optical Propagation Using Sinc Approximation," *Journal of the Optical Society of America A*, vol. 39, no. 8, pp. 1403-1413, 2022.

[15] D. Wegner, "Imaging Simulation Of Atmospheric Turbulence Based On Phase Screen Methods," *Ph.D. thesis, Institut für Meteorologie und Klimaforschung – Atmosphärische Spurenstoffe und Fernerkundung (IMK-ASF)*, pp. 75-83, 2022.

[16] R. N. Hassan, "Computer Simulation Of Segmented Mirrors For Large Optical Telescopes," *Ph.D. thesis, university of Baghdad-College of science, Iraq-Baghdad*, pp. 35-36, 2012.

[17] A. Glindemann, S. Hippler, T. Berkefeld, and W. Hackenberg, "Adaptive Optics on Large Telescopes," *Experimental Astronomy*, vol. 10, pp. 5–47, 2000.

[18] D. Baiocchi, and J. H. Burge, "Radius of Curvature Metrology for Segmented Mirrors," *Proceedings of the SPIE- The International Society for Optical Engineering*, vol. 4093, pp. 58-67, 2000.

[19] R. Francois, "Adaptive Optics in Astronomy," *Cambridge university press*, pp. 239-246, 1999.

[20] T. R. Rimmele, K. Richards, S. L. Hegwer, D. Ren, S. Fletcher , S. Gregory, L. V. Didkovsky, C. J. Denker, W. Marquette , J. Marino, and P. R. Goode, "Solar Adaptive Optics: A Progress Report," *Adaptive Optical System Technologies II*, vol. 4839, pp. 635-646, 2003.

[21] https://solarsystem.nasa.gov/resources/764/prominence-from-the-solar-dynamics-observatory/

[22] D. Schmidt, T. Rimmele, J. Marino, and F. Wöger, "A Review of Solar Adaptive Optics," *Proceedings of the SPIE*, vol. 9909, id. 99090X 8, pp. 8-16, 2016.

[23] C. Li, Y. Lu, and S. Zhang, "Direct Wavefront Sensing From Extended Objects: A General Sensor," *Optical Engineering*, vol. 60, no. 7, pp. 073107- 073124, 2021.

[24] M. Hart, and J. L. Codona, "Wavefront Sensing with the Differential Optical Transfer Function," *Unconventional Imaging and Wavefront Sensing*, vol. 8520, pp. 852-836, 2012.

[25] J. M. Beckers, "Adaptive Optics for Astronomy: Principles, Performance And Application," *Annual Review of Astronomy and Astrophysics*, vol. 31, pp. 55-56, 1993.

[26] P., F. Quir´os, "Reconstruction and Control Laws for Multi-conjugate Adaptive Optics in Astronomy," *Ph.D. thesis, imperial college London*, pp. 62-63, 2007.

[27] S., Ströbele M. Kasper, and P. Y. Madec, "Overview on Wavefront Corrector Technologies for Astronomy and Solar Adaptive Optics Systems," *Proceedings of the SPIE*, vol. 11448, id. 114481B, pp. 13-26, 2020.

[28] R. N. Hassan, H. S. Ali, and W. H. Wadee, " Computer Simulation for the Effects of Optical Aberrations on Solar Images Using Karhunen-Loeve polynomials," *Iraqi Journal of Science*, vol. 62, no. 7, pp. 2463-2473, 2021.

[29] L. K. Abood, S. M. Al-Hilly, and R. N. Hassan, "Describing the Wavefront Aberrations of the Hexagonal Aperture Using Modified Zernike Polynomials," *Iraqi Journal of Science*, vol.54, no.1, pp.222-231, 2013.

[30]U. E. Jallod, "Simulations of Four Types of Optical Aberrations using Zernik Polynomials," *Iraqi Journal of Science*, vol. 58, no. 1C, pp.583-591, 2017.

[31] N. Chimitt, and S. H. Chan, "Simulating Anisoplanatic Turbulence by Sampling Inter-modal and Spatially Correlated Zernike Coefficients," *Optical Engineering*, vol. 59, no. 8, pp. 83101-83127, 2020.